Effects of boundaries and density inhomogeneity on states of vortex matter in Bose-Einstein condensates at finite temperature

Effects of boundaries and density inhomogeneity on states of vortex matter in Bose–Einstein condensates at finite temperature

S. Kragset[1], E. Babaev[2,3], and A. Sudbø[1,4]
[1] *Department of Physics, Norwegian University of Science and Technology, N-7491 Trondheim, Norway*
[2] *Physics Department, University of Massachusetts, Amherst, 01003-9337, USA*
[3] *Department of Theoretical Physics, The Royal Institute of Technology 10691 Stockholm, Sweden*
[4] *Center for Advanced Study, The Norwegian Academy of Science and Letters, Drammensveien 78, 0271 Oslo, Norway*

Most of the literature on quantum vortices predicting various states of vortex matter in three dimensions at finite temperatures in quantum fluids is based on an assumption of an extended and homogeneous system. It is well known not to be the case in actual Bose–Einstein condensates in traps which are finite systems with nonuniform density. This raises the question to what extent one can speak of different aggregate states of vortex matter (vortex lattices, liquids and tensionless vortex tangle) in these system. To address this point, in the present work we focus on the finite-size, boundaries and density inhomogeneity effects on thermal vortex matter in a Bose–Einstein condensate. To this end we perform Monte Carlo simulations on a model system describing trapped Bose–Einstein condensates. Throughout the paper, we draw on analogies with results for vortex matter obtained for extended systems. We also consider, for comparison, the cylindrical confinement geometry with uniform density profile from the center out to the edge of the trap. The trapping potential is taken to be generically of an anharmonic form in such a way as to interpolate between a harmonic trap and a cylindrical confinement geometry. It also allows for a dip in the density profile at the center. We find distinct thermal equilibrium properties of the vortex system as the qualitative characteristics of the trapping potential is varied. For a uniform cylindrical confinement geometry, we find a vortex lattice at the center of the trap as well as ring-like thermal fluctuations of the vortex system as the trap edge is approached. For a harmonic trap, we find a distinct region at the edge of the trap where the vortex lines appear to have lost their line tension. Due to the steep density gradient, this crosses directly over to a vortex-line lattice at the center of the trap at low temperatures. At higher temperatures, an intermediate tensionful vortex liquid may exist. For an anharmonic trap where the ground state condensate density features a local minimum at the center of the trap, we find a corresponding region which appears to feature a tensionless vortex-line liquid phase. This work suggests that finiteness and intrinsic inhomogeneity of the system not withstanding, one nonetheless can approximately invoke the notion of distinct aggregate states of vortex matter realized at certain length scales. This might be helpful, in particular in search of possible new states of vortex matter in Bose–Einstein condensates with multiple components and different symmetries.

PACS numbers: 03.75.Hh,03.75.Kk,67.40.Vs

I. INTRODUCTION

The physics of trapped gases on the one hand, and the physics of superconductors and superfluids on the other, may be conceptually linked by rotating Bose–Einstein condensates (BEC) in magnetic traps[1], or pair condensates of ultracold Fermi gases[2,3,4]. Superconductivity, superfluidity, and Bose–Einstein condensation are all hallmarks of quantum fluids governed by the onset of long-range phase coherence in a macroscopic matter wave. This phase-coherence is the matter-wave analog of a corresponding well-known phenomenona in electromagnetic waves, namely phase-coherence in such waves established by stimulated emission of radiation. One distinguishing feature of such quantum fluids is that the macroscopic matter wave function is complex $\psi(r) = |\psi(r)|e^{i\theta(r)}$, and with a phase $\theta(r) \in [0, 2\pi\rangle$, i.e. this phase is defined with a compact support. This has far-reaching ramifications for the physics in the sense that the order parameter of the system supports stable topological defects in the form of point-vortices in two dimensions and vortex-loops and vortex-lines in three dimensions. Phase transitions from superfluids to normal fluids, are entirely governed by such topological defects.

In two dimensions, this is manifested in the well known Kosterlitz–Thouless phase transition of unbinding of a vortex-antivortex pair from a low-temperature superfluid with only tightly bound vortex-antivortex pairs to a normal fluid in a process where the most weakly bound pairs are dissociated[5]. It is also equivalent to a phase transition from a dielectric to a metal in the two-dimensional Coulomb-gas with overall charge-neutrality[6]. In three dimensions, one has a phase-transition from an ordered low temperature phase with at most a few small closed vortex loops present, to a normal fluid where closed vortex loops have proliferated throughout the system into a tangle in such a way as to make it possible to connect opposite sides of a macroscopic system with a connected vortex path[7,8,9,10,11,12]. This was originally proposed by Onsager already in 1949 in qualitative terms as a way of explaining the λ-transition in superfluid ^{4}He[13]. In the context of the present paper, we stress that while Refs.

7,13 dealt with the issue for zero rotation for the superfluid or zero magnetic field for the superconductor, the picture was extended to finite rotation in superfluids and finite magnetic field in extreme type-II superconductors in Refs. 8,9,10. It is the latter situation that is relevant to rotating Bose–Einstein condensates.

The connectivity of the thermally excited vortex tangle changes abruptly at the critical temperature of the system. Such a phase transition in three dimensions cannot be cast into the framework of a Kosterlitz–Thouless phase transition for the simple reason that vortex loops in three dimensions have a property that vortex-antivortex pairs in two dimension do not have, namely shape. This contributes significantly to the configurational entropy of the system. The fact that vortex loops can have extremely complicated geometric shapes and will form a fractal structure at long length scales at the critical point, is crucial in order for them to be able to proliferate. It also means that the vortex loops cannot be regarded as renormalized vortex rings with a 'doughnot hole' in the middle. They are instead fractal objects with fractal dimension $D_H \approx 2$[14]. Such a fractal dimension is considerably larger than what it would have been for ring-like objects, namely $D_H = 1$. The entropy production associated with this proliferation of topological defects is accompanied by a loss of a generalized stiffness, in this case the superfluid density or phase stiffness of the system. In this sense, the above scenarios both in 2D and 3D fall nicely within a general definition of a phase transition, namely that a phase transition occurs at a point where some generalized stiffness is lost as a result of a spontaneous proliferation of stable topological defects of the complex scalar matter fields in the system[15].

Over the last decade, remarkable progress has been made in achieving Bose–Einstein condensates in gases of ultra-cold atoms in a magnetic trap[16,17,18]. Such condensates are now being routinely manipulated in a large variety of ways, and may for instance be spun up to produce vortex lattices of a condensate in a magnetic trap[19,20]. One may also envisage low-dimensional vortex structures[21,22]. There are even cases where other aggregate states of vortex matter are known to exist in quite different condensed matter systems, such as two-component superconductors with individually conserved condensates[24]. It is the purpose of this paper to study the thermal excitations of vortex-lines and vortex-loops in Bose–Einstein condensates which are confined to a cylindrical geometry by a trapping potential. This trapping potential generally increases from the center of the trap towards the edge of the condensate, although this variation may be non-monotonic. In essence, it acts as a spatially dependent chemical potential for the bosons in the system, thus affecting the overall condensate density. The density is typically highest at the center of the trap and vanishes towards the edge of the trap, although more complicated profiles may easily be envisaged, and will in fact be considered in this paper. The way in which the overall density varies is directly determined by the trapping potential. Thus, such systems are inherently nonuniform and therefore it is important specifically to study the effect of spatial density variations.

This paper is organized as follows. In Section II, we motivate and introduce the model on which we will perform Monte Carlo simulations in this paper. In Section III, we describe the Monte Carlo simulations we will perform. In Section IV we present results for a uniform system, as a benchmark, and we also consider such a system confined in a cylindrical geometry. The former of these results are applicable to fluctuating vortex matter in extreme type-II superconductors, where we can neglect the fluctuations in the gauge field. The latter results apply to rotating helium in a container. In Section V we present our results for two different types of traps, namely the harmonic cylindrical trap, and the anharmonic cylindrical trap. The quantities we focus on are the helicity modulus and structure functions of the vortex matter in the systems in the various parts of the confinement and traps, i.e. at various distances from the center. In Section VI we present our conclusions. This work is a follow-up of the letter Ref. 25.

II. GENERAL MODEL

We will use Monte Carlo (MC) computations to search for the thermal equilibrium vortex states of a rotating Bose–Einstein condensate in three dimensions. A natural starting point is the Gross-Pitaevskii free energy functional in a rotating frame, given by the energy functional

$$E' = \int dV \Big[\psi^* (-\frac{\hbar^2}{2M}\nabla^2 + V(r) - \Omega \hat{L}_z)\psi + \frac{1}{2} g|\psi|^4 \Big]. \quad (1)$$

Here, $\hat{L}_z = \mathrm{i}\hbar(y\partial_x - x\partial_y)$ and $g = 4\pi a_s \hbar^2/M$, M is the mass of the atoms in the condensate, and a_s is the s-wave scattering length. The condensate wave function is given by $\psi(r) = \sqrt{\rho(r)}e^{i\theta(r)}$, where $\rho(r)$ is the local density of the bosonic matter in the trap. Long-range ordering in the phase variable $\theta(r)$ signals the onset of superfluidity or Bose–Einstein condensation. It will be important for our later discussion that, consequently and conversely, the *destruction* of the Bose–Einstein condensate proceeds via phase-disordering of the system through large phase fluctuations $\nabla\theta$. Here, "large" means phase fluctuations that give rise to vortices due to the compact nature of the phase variable $\theta \in [0, 2\pi\rangle$, i.e. phase fluctuations that have the property $\nabla \times (\nabla\theta) = 2\pi\mathbf{n}$, where $\mathbf{n}$ is an integer-valued vector. These are the *transverse* phase fluctuations, as opposed to the *longitudinal* ones, which correspond to spin-waves in an XY ferromagnet.

The potential $V(r)$ is a trapping potential which confines the Bose–Einstein condensate in a finite region in space. Moreover, it is also seen to appear as a spatially varying chemical potential for the condensate density and as such will set the overall density profile of the condensate. Increasing $V(r)$ will suppress the condensate

density and vice versa. Furthermore, Ω is the angular frequency associated with the rotation of the condensate when it is spun up, and $\hat{L}_z$ is the corresponding total angular momentum operator. Finally, the quartic term is a repulsive contact interaction between the bosons of the condensate which will render the spectrum of the theory bounded from below. Such an energy functional is applicable as a coarse grained description of an uncharged phase coherent condensate[26].

If we formally introduce a vector potential $\mathbf{A} = (M/\hbar)(\mathbf{\Omega} \times \mathbf{r})$ with $\mathbf{\Omega} = \Omega\hat{\mathbf{z}}$, the energy functional in Eq. (1) can be written

$$E' = \int dV \Big[-\frac{\hbar^2}{2M}\psi^*(\nabla - \mathrm{i}\mathbf{A})^2\psi + \Big(V(r) - \frac{1}{2}M\Omega^2 r_\perp^2\Big)|\psi|^2 + \frac{1}{2}g|\psi|^4\Big], \tag{2}$$

where $r_\perp^2 = x^2 + y^2$. This is formally similar to the Ginzburg–Landau free energy of a superconductor, apart from the position-dependent term involving the trapping potential $V(r)$ and rotation Ω. However, in a superconductor the vector potential $\mathbf{A}$ has dynamics and is related to the magnetic field $\mathbf{B}$ by $\mathbf{B} = \nabla\times\mathbf{A}$, and thus we would normally include a term $(1/2\mu_0)B^2$ in the free energy density. For extreme type-II superconductors where the typical penetration depth λ_L of a static magnetic field is much larger than the coherence length ξ, fluctuations in the magnetic field can in many cases be ignored and this term in the energy can be dropped. The similarity of the superconductor Ginzburg–Landau theory to that of a rotating Bose–Einstein condensate is then striking.

So far, the energy functional of Eq. (2) is a continuum theory, but for the purposes of carrying out computer computations, it is more convenient to discretize space into a lattice and to rescale the wave function to avoid prefactors. That is, we let the wave function $\psi(\mathbf{r}) \to (\sqrt{M}/\hbar)\psi_i$, so that it is only defined on vertices $i = 1, \ldots, L^3$, separated by a lattice constant a. We also replace the gradient term with a gauge invariant lattice difference,

$$\psi^*(\nabla - \mathrm{i}\mathbf{A})^2\psi \to \sum_\mu |\psi_{i+a\mu}\mathrm{e}^{-\mathrm{i}A_{i\mu}} - \psi_i|^2. \tag{3}$$

$i + a\mu$ is the lattice site situated next to site i in direction μ, and the gauge field $A_{i\mu}$ here lives on the links of the lattice and it is given by the line integral

$$A_{i\mu} = \int_i^{i+a\mu} \mathrm{d}l A_\mu. \tag{4}$$

The continuum theory is recovered if we let $a \to 0$.

For high-T_C superconductors, where $\lambda_L \gg \xi$, it is a well established approximation only to consider fluctuations in the phase of the order parameter. This is frequently referred to as the London approximation[27], in which we simply assume a condensate of Cooper pairs to exist by having a finite and fixed $|\psi_i| = |\psi|$, since in the end, it is not the depletion of the number of Cooper pairs that is responsible for destroying superconductivity, but rather the proliferation of vortex loops originating with violent transverse phase fluctuations in the superconducting order parameter[8,10]. High-T_C superconductors are extreme type-II superconductors, which in a certain sense means that the (renormalized) charge of the condensate is small[8,10]. This suppresses gauge field fluctuations and an external magnetic field therefore only acts as a frustration on the system via minimal cupling to a fixed external vector potential, just as in the above Eq. (2). Superfluids and Bose–Einstein condensates have zero charge and may in this sense be viewed as the ultimate extreme type-II superconductors where all vestiges of the fluctuating gauge field in the problem have vanished. In these systems we therefore expect that the phase only approximation is essentially exact. Increasing the temperature, large fluctuations in the phase θ makes the condensate incoherent and non-superconducting before $|\psi|$ vanishes, see for instance Fig. 1 of Ref. 10. In fermionic pair condensates[28,29], it has been strikingly demonstrated that one may have pairing without superfluidity[30,31,32,33], providing further confirmation of the above ideas in a completely different setting than extreme type-II superconductors or ^{4}He[13].

The right hand side of Eq. (3) can be rewritten

$$|\psi_{i+a\mu}\mathrm{e}^{-\mathrm{i}A_{i\mu}-\psi_i}|^2 = |\psi|^2[2 - 2\cos(\Delta_\mu\theta_i - A_{i\mu})], \tag{5}$$

using the lattice difference operator $\Delta_\mu\theta_i = \theta_{i+a\mu} - \theta_i$. A slight generalization is instead to replace $\psi_{i+a\mu}$ and ψ_i in Eq. (3) with their average as this will allow for a *non-uniform condensate density*, which is what we want to study here.

Since we will only include phase fluctuations in the Monte Carlo computations, any terms *not* containing θ will represent mere constant shifts in the total energy and we will consequently drop them. We thus arrive at a simple, effective energy

$$E = \sum_{i\mu} P_{i\mu}\cos(\Delta_\mu\theta_i - A_{i\mu}). \tag{6}$$

The sum is over all positions and directions x, y, z, and except for a factor $M/\hbar^2$, the position dependent coupling $P_{i\mu}$ is nothing but the condensate density at the link from site i in μ-direction. If this factor is set to unity, Eq. (6) reduces to the well known uniformly frustrated 3D XY model, used for modelling the melting of the vortex-line lattice in uniform bosonic condensates and extreme type-II superconductors (see e.g. Refs. 34,35,36,37,38). The local vorticity can be calculated from a phase configuration by summing the gauge-invariant phase difference around each plaquette in the numerical grid,

$$\sum_{\square_j}(\Delta_\mu\theta_i - A_{i\mu}) = 2\pi n_j. \tag{7}$$

Here, n_j is the number of vortices penetrating a plaquette $\square_j$ in the positive direction. The spatial (radial) variation of $P_{i\mu}$ reflects directly the spatial variation *in the*

ground state of the system of the quantity $|\psi(r)|^2$ due to the spatial variation of the effective chemical potential $V(r) - \frac{1}{2}M\Omega^2 r_\perp^2$ appearing in Eq. (2).

We mention in passing that *longitudinal* phase fluctuations are innocuous in 3D, and hence need not be considered for the purposes of studying phase transitions in the system. Such phase-fluctuations are incapable of destroying the superfluid density in 3D. In 2D they suffice to render the system *critical* at any finite temperature below the Kosterlitz–Thouless transition, meaning that phase-correlations $G(\mathbf{r}-\mathbf{r}') \equiv \langle e^{i\theta(\mathbf{r})}e^{-i\theta(\mathbf{r}')}\rangle$ exhibit a quasi-long range *power-law* decay $G(r) \sim 1/r^\eta$ with a temperature-dependent exponent η. In neither case are longitudinal phase fluctuations capable of driving the system *through* a phase transition and into a phase with short-range, *exponentially* decaying phase-correlations $G(r) \sim e^{-r/\xi}$, where ξ is the correlation length.

It should be noted that the model Eq. (6) does not apply to the Lowest Landau Level regime (LLL) of an atomic Bose–Einstein condensate. The latter can be identified through the ratio of the interaction energy scale to the level spacing of the transverse harmonic confinement in an axially symmetric trap,

$$\lambda = \frac{4\pi\hbar^2 a_s n}{M\hbar\omega_\perp}, \tag{8}$$

where n is the particle number density, a_s is the s-wave scattering length, M is the particle mass and $\omega_\perp$ is the trap frequency. The LLL approximation is considered to be valid when $\lambda \ll 1$[40,41]. However, we expect Eq. (6) to be adequate under the conditions of those experiments which meet the following naive requirement. The intervortex distance $2r_0 = 2\sqrt{\hbar/M\Omega}$ should be substantially larger than the healing (or coherence) length $\xi = \hbar/M\omega_\perp R_\perp$, where $R_\perp$ is the radius of the system perpendicular to the axis of rotation[42,43,44,45,46,47].

III. MONTE CARLO COMPUTATIONS

The Monte Carlo computations are performed with the standard Metropolis-Hastings algorithm[48,49], and the updates are always local. Initially, all phases are chosen equal to zero, but any other configuration would suffice, provided that the system is allowed to thermalize for a sufficiently long time. We then proceed systematically through all lattice sites one by one and propose trial updates of the local phases $\theta_i \to \theta_i + \delta\theta_i$, where $\delta\theta_i$ is drawn from a uniform distribution $[-\pi, \pi\rangle$. Each trial update is accepted with a probability p determined from the energy difference ΔE of the configurations before and after the update,

$$p = \begin{cases} 1 & \text{if } \Delta E < 0, \\ \mathrm{e}^{-\Delta E/T} & \text{if } \Delta E \geq 0. \end{cases} \tag{9}$$

The result is a Markov chain of configurations that can be used to estimate the partition function

$$Z = \sum_{\{\theta\}} \mathrm{e}^{-E/T}, \tag{10}$$

where the sum is over all possible sets of the phase. An obvious effect of generating phase configurations according to the Boltzmann distribution is how the amount of fluctuations is controlled by the temperature T. At high temperatures, the phases will fluctuate more easily whereas they tend to freeze when T is lowered. In this paper, we will use units of temperature that are such that the critical temperature of the model in Eq. (6), with $P_{i\mu} = 1$ and $A_{i\mu} = 0$, is $T_C \simeq 2.2$. By inspecting the energy Eq. (6) we see that in a Monte Carlo computation, the density profile $P_{i\mu}$ effectively works as the inverse of a position dependent effective temperature, such that

$$T_{\text{eff}} = \frac{T}{P_{i\mu}}, \tag{11}$$

whence we expect phase fluctuations to depend strongly on the density profile of the condensate. This is an exact statement within the phase-only approximation. In particular, this means that the trapped condensates effectively are "warm" (in the sense of being close to the condensation temperature) wherever the ground state density is low. In regions of low density we therefore expect more violent vortex fluctuations. As will be shown below, this is typically the case close to the edge of the trap, but may also be true close to the center of the trap for anharmonic trapping potentials with a dip in the condensate density at the center of the trap.

We define the process of going over all sites once as one sweep and measure the Monte Carlo time in units of the sweeps. Initially at each temperature, all realizations of the system are thermalized with at least 100 000 sweeps to make sure they fluctuate around the equilibrium state before any measurements are made. To calculate thermal averages, we sample the configuration every 100th sweep. The numerical grid is cubic with a linear extension $L = 72$ (for the case of the uniform cylinder, we also consider $L = 36$).

A. The helicity modulus

Phase coherence in a vortex system is probed by computing the helicity modulus Υ_μ, equivalently the *superfluid density*, defined as the change in free energy $F = -T \ln Z$ as a result of a phase twist $\tilde{\mathbf{\Delta}}$ applied in the the following way,

$$E[\tilde{\mathbf{\Delta}}] = \sum_{i\mu} P_{i\mu} \cos(\Delta_\mu \theta_i - A_{i\mu} - \tilde{\Delta}_\mu). \tag{12}$$

The expansion of the free energy is even in $\mathbf{\Delta}$, which can be viewed as a change in the boundary conditions of

the system. For small deviations from periodic boundary conditions, the leading behaviour is quadratic and the helicity modulus is given as the coefficient to the second order term,

$$\begin{aligned}\Upsilon_\mu &\equiv \frac{1}{L^3}\left.\frac{\delta^2 F}{\delta\tilde{\Delta}_\mu^2}\right|_{\tilde{\Delta}_\mu=0} \\ &= \frac{1}{L^3}\left\langle \sum_i P_{i\mu}\cos(\Delta_\mu\theta_i - A_{i\mu})\right\rangle \\ &- \frac{1}{TL^3}\left\langle\left[\sum_i P_{i\mu}\sin(\Delta_\mu\theta_i - A_{i\mu})\right]^2\right\rangle. \quad (13)\end{aligned}$$

The twist can be applied in any direction, and without rotation the response in terms of Υ_μ is equal for all $\mu = x, y, z$. When the temperature is increased from low to high, thermal fluctuations gradually destroy phase coherence. Consequently, the renormalized superfluid density continuously evolves from a finite value to zero at some critical temperature. On the other hand, in a rotating system the helicity modulus will be different for the x- and y-directions than along the axis of rotation. Both cases are however important since Υ_x and Υ_y carries information on numerical pinning. In the computations, we choose the vector potential so that $\nabla \times \mathbf{A} = (0, 0, 2\pi f)$, where f is the number of rotation-induced vortices per numerical grid-plaquette in the xy-plane. For technical reasons, we restrict the filling fraction $f \leq k/L^2$ with $k = 1, 2, 3, \ldots$, but at the same time the density of vortex lines should not be too high in order to avoid artificial pinning to the underlying numerical grid[50]. This can be probed by the helicity modulus in the transverse directions. A zero value of Υ_x and Υ_y means that the vortex line lattice is free to move translationally with respect to the grid. For very low temperatures, there will always be pinning, but the pinning should disappear well below the temperature at which the lattice melts. This melting on the other hand, is characterized by a discontinuous jump in the superfluid density measured parallel to the vortex lines, i.e. a jump in Υ_z to zero.

In non-uniform systems, we encounter a problem with the above definition of the helicity modulus, since $P_{i\mu}$ equal to or close to zero at the system edges will favour fluctuations at all temperatures in these regions. The global Υ_μ mixes together information on the amount of fluctuations in all regions, and the interpretation is therefore less useful. To obviate this difficulty, we introduce a modified helicity modulus in z-direction, defined in a selected region between two cylinders of radii R_1 and R_2. We do so by applying a twist

$$\tilde{\mathbf{\Delta}}(r_{iz}) = \begin{cases}\tilde{\Delta}\hat{\mathbf{z}} & \text{if } R_1 \leq r_{iz} < R_2, \\ 0 & \text{otherwise,}\end{cases} \quad (14)$$

and defining the modified helicity modulus as follows,

$$\begin{aligned}\tilde{\Upsilon}_z(R_1, R_2) &\equiv \frac{1}{N'}\left\langle {\sum}' P_{iz}\cos(\Delta_z\theta_i - A_{iz})\right\rangle \\ &- \frac{1}{TN'}\left\langle\left[{\sum}' P_{iz}\sin(\Delta_z\theta_i - A_{iz})\right]^2\right\rangle. \quad (15)\end{aligned}$$

Here, $\sum'$ is over all sites where $\tilde{\mathbf{\Delta}}(r_{iz})$ is nonzero (depending on R_1 and R_2) and N' is the number of these sites. The local $\tilde{\Upsilon}_z(R_1, R_2)$ provides a measure of the phase coherence more locally than the global quantity, and will therefore be used to investigate the character of the vortex state at different positions in a trapped Bose–Einstein condensate.

IV. UNIFORM SYSTEMS

As a warmup to the results to be presented below, we first consider two cases of uniform systems, namely the infinite uniform system and a cylindrical confinement geometry with uniform density. The former in particular allows connections to be made to the vast literature on vortex physics of extreme type-II superconductors such as high-T_C superconductors.

A. Infinite uniform system

We begin with a review of the Monte Carlo results for a uniform system, i.e. with $P_{i\mu} \equiv 1$ in Eq. (6), and we first consider the non-rotating case. This is the standard uniform 3D XY model, which has been studied extensively elsewhere, see for example Ref. 34,35,36,37,38. At low temperatures, the phases tend to align as spins in a ferromagnet, and the system is frozen in a stiff state where any change in boundary conditions is associated with a large response in free energy. Consequently, the helicity modulus is close to unity. Equivalently, the superfluid density is close to the ground state density $P_{i\mu}$. In Fig. 1 is shown the helicity modulus Υ_z along the z-direction, but Υ_x or Υ_y would give similar results. As the temperature is increased, the relevant phase fluctuations start to appear as vortex loops, in numbers that gradually increase with temperature. This reduces the superfluid density. However, not until the vortex loops loose their line tension (free energy per unit length) at the critical temperature $T_C \simeq 2.2$, will Υ_z vanish completely. The phase transition is continuous and accompanied by a diverging length scale in the thermodynamic limit and a developing singularity in the specific heat C_V as shown in Fig. 1. High precision measurements of the critical exponents can be found in Ref. 51

In the second row of Fig. 1, we show some snapshots from the computations where the vortices have been calculated via Eq. (7) and plotted in a 3D volume. The vortex radius is *chosen* to be 0.4 times the grid spacing for a convenient visualization, and this should not be

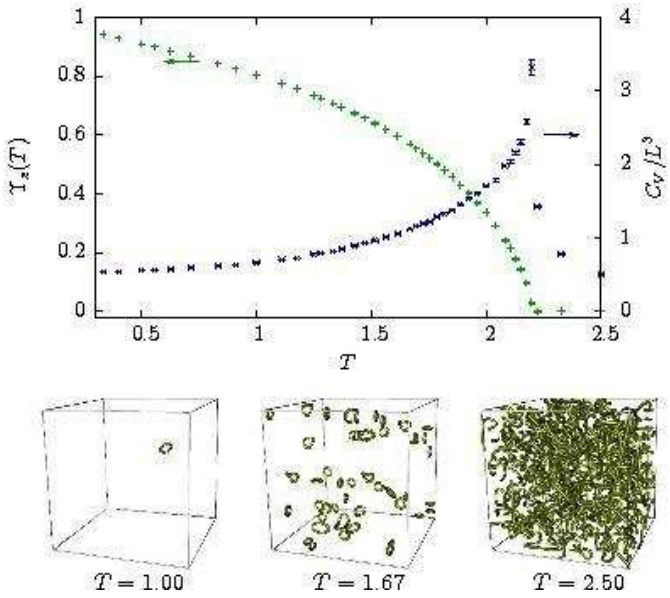

FIG. 1: (Color online) Monte Carlo results for a uniform system with periodic boundary conditions. The helicity modulus (superfluid density) Υ_z along the z-direction is plotted (+), but Υ_x and Υ_y give equal results. The specific heat C_V/L^3 ($\times$) has a peak at T_C, where Υ_z vanishes. In the second row, random snapshots of the vortex configurations are shown for three temperatures. These are sections with 16^3 lattice sites cut out from the 72^3 system.

associated with the true core size. Additionally, the vortices (especially the vortex *lines* in the rotating system we present below) exhibit sharp bends at short length scales. These bends result from the numerical grid. In fact, the vortices shown in the images are splines; the precise form of the vortices in the computations is straight line segments connected in perpendicular corners. Nevertheless, the model has proved to be accurate for vortex fluctuations at scales larger than the grid spacing[34,35,36,37,38]. Hence, the 3D snapshots provide useful hints to the state the system is in at different temperatures. Only occasional and small vortex loops appear when the temperature is low, but eventually they fill the whole volume. Above T_C, the system is in a state dominated by a tangle of tensionless vortex loops of all sizes, and there is no phase coherence or superfluidity.

In a rotating system, the scenario is different. The ground state is the famous Abrikosov lattice[52,53], where straight rotation-induced vortex lines arrange themselves in a triangular pattern, though with some defects due to the incommensurable underlying square numerical grid. Here, we present computation results from a system with filling fraction $f = 1/36$, and the structure of the vortex line lattice can be seen in Fig. 2. In the upper row is shown the structure function,

$$S(\mathbf{k}_\perp) = \frac{1}{fL^3}\left\langle \left| \sum_{\mathbf{r}_\perp} n(\mathbf{r}_\perp) \mathrm{e}^{\mathrm{i}\mathbf{k}_\perp\cdot\mathbf{r}_\perp} \right|^2 \right\rangle, \qquad (16)$$

where $n(\mathbf{r}_\perp)$ is the local vorticity given by Eq. (7) and the sum runs over the positions of all plaquettes in the xy-planes. The $\mathbf{r}_\perp$- and $\mathbf{k}_\perp$-vectors are perpendicular to the axis of rotation. The structure function exhibits sharp peaks for the characteristic Bragg vectors of the vortex line lattice when the temperature is low and the system close to its ground state. As the effect of thermal fluctuations sets in and the vortex lines gets more prone to bending, the Bragg-peaks are weakened, and eventually there is a transition from a sixfold-symmetric structure to a ring structure in $S(\mathbf{k}_\perp)$. This is the hallmark of a vortex liquid phase where the vortices still posess a line tension which disappears in a crossover transition at an even higher temperature. The second row in Fig. 2 is the real-space equivalent of the above, where the local vorticity $n(\mathbf{r}_\perp)$ is integrated along the z-direction so that closed vortex loops will be cancelled or averaged out. Both the Fourier- and real-space versions of the structure function are thermal averages calculated from 100 000 Monte Carlo sweeps. In the left panels of the second row, bright spots correspond to straight lines in relatively stable positions. Higher temperatures result in increased bending of the lines, and the bright spots develop into smeared-out regions until it is no longer possible to distinguish individual vortex lines in the rightmost panel. Insight into the bending mechanism can be obtained from the 3D sections in the third row, which are snapshots corresponding to those of the non-rotating case in Fig. 1. In principle, such snapshots from a Monte Carlo computation could produce *any* possible configuration, but a state far from equilibrium is highly unlikely. We therefore assume the pictures to be representative and useful indications of the system's state at a given temperature. Compared to the non-rotating system, we see that there is much going on in terms of vortex fluctuations even at low temperatures like $T = 1.00$, in the units we defined below Eq. (10). The energy cost associated with elementary vortex excitations, i.e. a closed vortex-loop, is less when there are vortex lines already present. A loop and a line can merge to produce a bend in the vortex line and enough bends will result in a melting transition at T_M. This is succeeded by a vortex loop blowout inside the vortex-liquid phase similar to what happens in the non-rotating case.

The qualitative picture above is supported by the qantitative measurements presented in Fig. 3. The vortex loop blowout no longer corresponds to a phase transition, but a remnant crossover is still indicated by a peak in the specific heat at a temperature $T > T_M$. A finite size scaling analysis would however reveal that there is no criticality associated with this broad peak[10]. On the other hand, the melting of the vortex line lattice is a first order phase transition characterized by a discontinuity

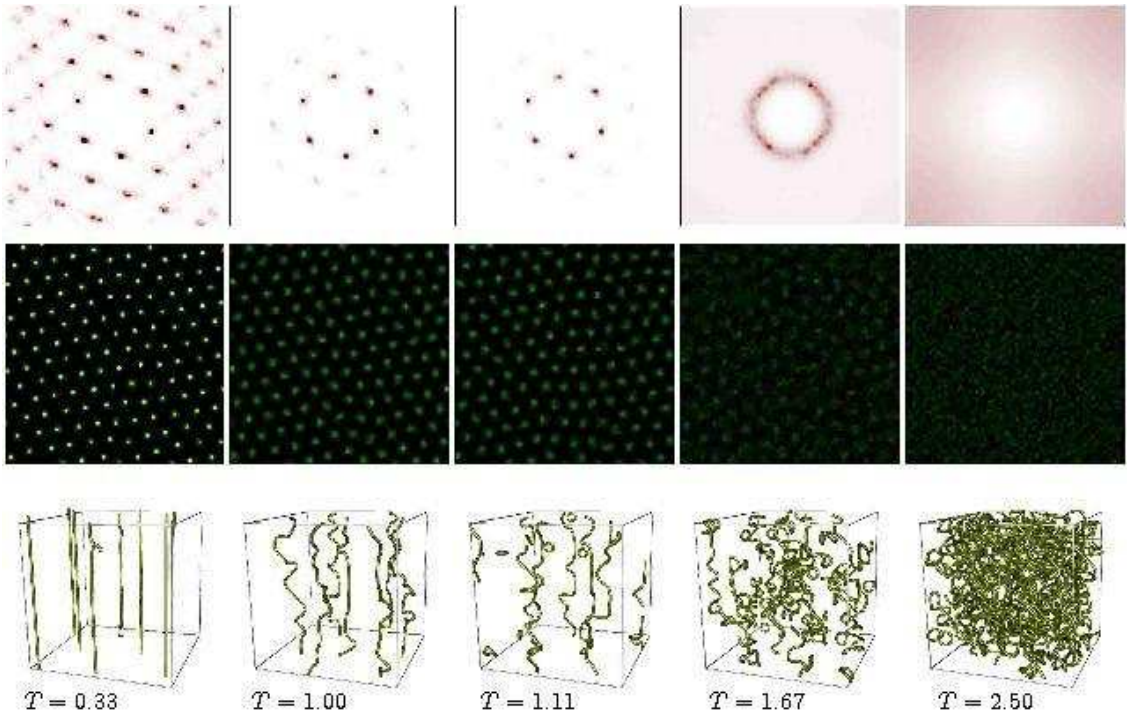

FIG. 2: (Color online) For each temperature, given below the columns, the structure function $S(\mathbf{k}_\perp)$ is shown in the upper row ($S(0)$ is removed, and in the two rightmost images the colorscale is magnified by a factor 25). There are sharp peaks for the characteristic Bragg vectors at the lowest temperatures before a transition to a ring structure corresponding to a vortex liquid phase at $T = 1.67$. In the second row we show the real-space equivalent to the structure function, the xy-positions of the vortices, integrated over z-direction. The averages of the first two rows are calculated from 100 000 Monte Carlo sweeps. In the third row, we show sections of size 16^3 from snapshots of the vortex configurations.

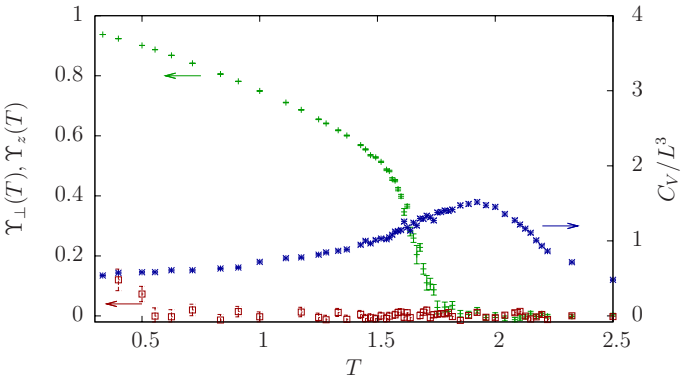

FIG. 3: (Color online) The helicity modulus Υ_z (+) along the axis of rotation is cut off and vanishes when the vortex lattice melts. In the transverse direction, a zero $\Upsilon_\perp = \Upsilon_x, \Upsilon_y$ (□) indicates that there is no pinning of the vortices to the numerical grid. The rounded peak in C_V/L^3 (×) is a remnant of the vortex-loop blowout transition in the non-rotating system.

in the helicity modulus (or superfluid density) Υ_z along the axis of rotation in the thermodynamic limit. In a finite system like the one we have simulated, the drop to zero is continuous, but compared to a non-rotating system, it is much steeper and takes place at a lower temperature. Finally, note that the helicity modulus in the transverse direction $\Upsilon_\perp$ is zero for temperatures well below the melting transition, indicating that the vortex line lattice is not pinned to the numerical grid.

B. Cylindrical container

We next consider the case of a uniform cylinder. This gives a ground state density profile $P_{i\mu}$ illustrated in Fig. 4. Figs. 5 and 6 show the results from computations of vortex matter in a cylindrical container with such a density profile, given by

$$P_{i\mu} = \Theta(r_{i\mu} - R), \tag{17}$$

where Θ is the Heaviside step function $\Theta(x) = 0, x < 0$; $\Theta(x) = 1, x > 0$. We have used two different system sizes L, but with the same filling fraction $f = 1/36$ to see how the radius $R = L/2 - 2$ affects the ordering of the vortices. At low temperatures, the computations reproduce orderings with circular distortions of the vortex line lattice near the container wall, as predicted for ^{4}He in a zero-temperature treatment of the problem[54]. For a large number of vortices the system reacquires the hexagonal lattice symmetry away from the wall, see Fig. 5 (bottom row). Increasing the temperature in the case of small

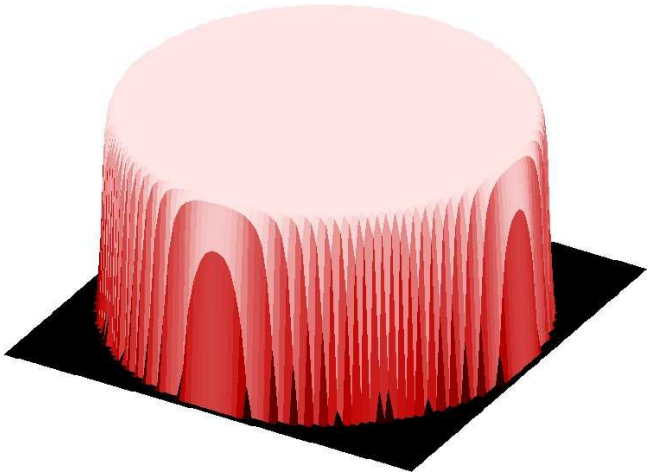

FIG. 4: (Color online) Radial density profile $P_{i\mu}$ for the case of a uniform sylinder. The density is uniform in the z-direction.

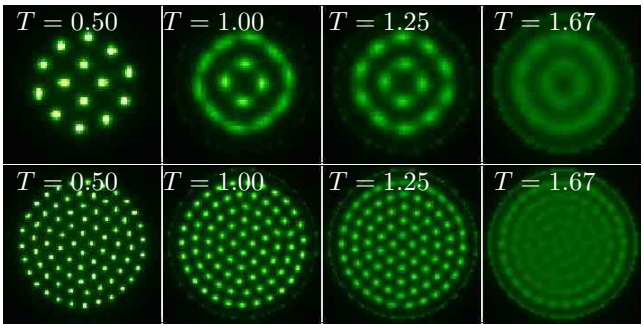

FIG. 5: (Color online) xy positions of vortices in a cylindrical container integrated over z-direction, and averaged over every tenth of a total of $5 \cdot 10^5$ MC sweeps. Top and bottom rows have $L = 36$ and $L = 72$, respectively. At $T = 0.5, 1.0$, we discern circular ordering close to the cylinder wall combined with a hexagonally ordered state closer to the center. At $T = 1.25, 1.67$ we observe dominance of angular fluctuations closest to the edge.

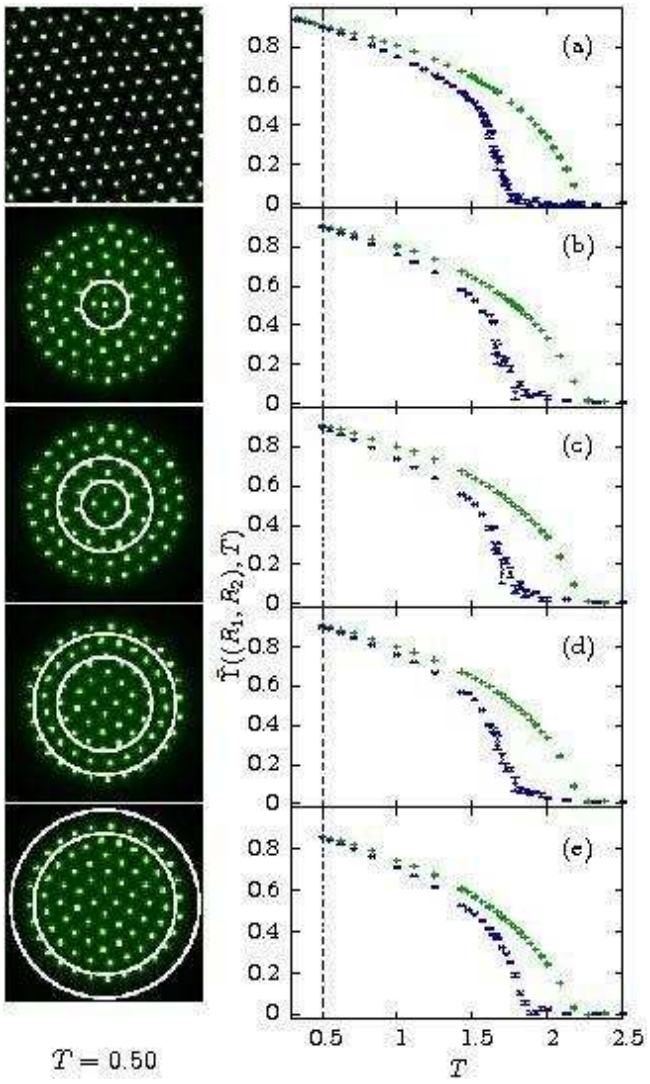

FIG. 6: (Color online) Results for $\tilde{\Upsilon}_z(R_1, R_2)$ in a cylindrical container. In panels (b)–(e) are shown the helicity moduli $\tilde{\Upsilon}_z(R_1, R_2)$ for radii $R_1, R_2 = 0, R/4, 2R/4, 3R/4, R$, as indicated by the white circles in the images on the left, and compared to the results for the extended uniform system, panel (a). The upper curve (+) is the helicity modulus without rotation, while the lower curve (×) is the results with rotation-induced vortices present (filling fraction $f = 1/36$). All regions in the cylindrical container behave almost as the uniform system.

number of vortices (top row of Fig. 5) the dominant vortex fluctuations are associated with angular displacements, while radially the vortex density remains ordered. For the largest system, with many vortices, (bottom row of Fig. 5) we find dominance of angular fluctuations only for the vortices situated close to container wall, while the center of the system does not display this phenomenon.

The crossover to a uniformly molten vortex system occurs in both cases only at a higher temperature. The two-step thermal crossover in the vortex pattern we find is analogous to that in two dimensions where vortices are point-like objects (see e.g. Ref. 55). There is, however, a principal difference in our case, since in three dimensions the vortex line lattice melting is accompanied by significant vortex bending fluctuations.

Inspecting the modified helicity modulus $\tilde{\Upsilon}_z(R_1, R_2)$ (Fig. 6) for different regions (R_1, R_2) inside the cylinder, and comparing these results to those of a uniform system (panel (a)), we find only small differences. The cylindrical system behaves as the uniform one, and the circular distortions do not seem to affect the superfluid density. One could argue that the drop to zero is a little more rounded in the rotating non-uniform system, but this can be explained by the fact that $\tilde{\Upsilon}_z(R_1, R_2)$ is calculated for smaller subsystems and that the finite size effects necessarily should be more severe here. In fact the cylindrical container is just a uniform system with different boundary conditions, and in a sufficiently large system the boundary effects are irrelevant.

V. NON-UNIFORM SYSTEMS

In this section we present Monte Carlo results from systems with non-uniform density profiles $P_{i\mu}$. The finite size of the systems is now a wanted feature and closer to the real situation with ultra-cold atoms, and we do not need to do finite size scaling. Strictly speaking, the only possibility for transitions are of crossover nature. To reduce the surface effects and because we model elongated systems, we employ periodic boundary conditions in the z-direction. Global quantities such as the ordinary helicity modulus Υ_μ and the structure function $S(\mathbf{k}_\perp)$ have no rigorous meaning in these systems, and we rather use local versions like the modified helicity modulus $\tilde{\Upsilon}_z(R_1, R_2)$ and the local vorticity $n(\mathbf{r}_\perp)$. The 3D snapshots are also useful indicators on the mechanisms involved.

A. Harmonic trap

For a system in a harmonic trap, we choose a density profile according to the Thomas–Fermi approximation[39,40,41] with the shape of an inverse parabola, $P_{i\mu} = P^h\left(\frac{r_{i\mu}}{R}\right)\ \Theta(R - r_{i\mu})$, where Θ is the Heaviside step function $\Theta(x) = 0, x < 0, \Theta(x) = 1, x > 0$, and

$$P^h(x) = 1 - x^2. \tag{18}$$

The density gradient in a trap can alternatively be viewed as an effective temperature gradient in a uniform system, see Eq. 11. It is clear that for low, but finite, actual temperatures T, there will be a finite area near the edge of the cloud which *effectively* would be at a high enough temperature to feature an annulus of tension-less tangle of vortices. This is a phase where the vortex line tension has vanished through the proliferation of vortex loops. The ground state density profile $P_{i\mu}$ is shown for the harmonic trap in Fig. 7. The question is whether there is

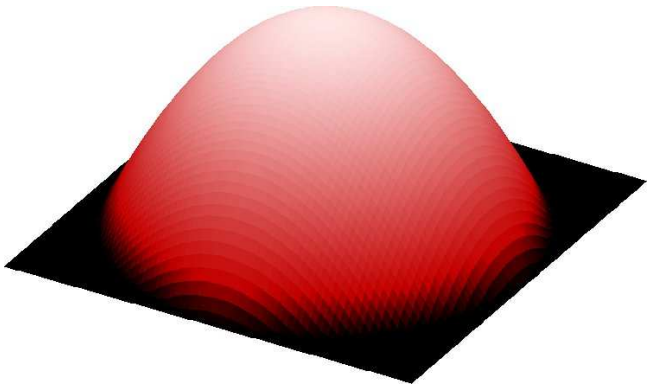

FIG. 7: (Color online) Radial density profile $P_{i\mu}$ for the case of a harmonic trap.

also a vortex liquid region in between the ordinary vortex line lattice and the tensionless annulus, which represents the true boundary of the condensate. The 3D snapshots in Fig. 8 illustrate how the vortices are stiffer in the central part than further out towards the edge where there is an annulus with a tangle of tension-less vortices. At the higher temperature on the right, this region has grown, but simultaneously the amount of bends in the vortex lines in the center has increased.

Further insight into the stability of the vortex line lattice can be obtained from the z-integrated vorticity in Fig. 9. The top row consists of snapshots and already here it is easy to separate the ordered lattice region from the disordered one, since straight vortex lines are seen as bright spots while bent vortices result in smeared spots or even smeared regions. This observation may be related to experiments, where at least for non-equilibrated vortex systems the z-integration renders vortices essentially indistinguishable[56,57]. We have used a filling fraction $f = 1/36$. Taking parameters from Ref. 58, and using $\Omega = (h/M)N_v/2\pi R^2$ where N_v is the number of vortices in the trap, we find $\Omega \sim 100$Hz. Since $\omega_\perp \sim 500$Hz[58], this puts us well outside the LLL regime.

We find that a well ordered vortex line lattice extends over most of the system at $T = 0.50$. Note also the absence of circular distortions for the vortices at the edge of the system, as opposed to the situation in the cylindrical container. At $T = 1.67$ we can still distinguish $2-3$ central vortices where the density is the highest in the snapshot. However, in the thermal averages of the second and third row these vortices are no longer possible to detect due to their thermally fluctuating positions. The thermal averages are created by averaging snapshots like the ones in the first row over 100 000 Monte Carlo sweeps in the second row and 500 000 sweeps in the third. Indeed, in a finite system, the averaging will eventually produce a complete smearing even in the center of the trap since there is only a finite energy barrier to translate or rotate even a perfect vortex line lattice. Signatures of this effect can be seen in the difference between the $T = 1.25$ pictures of the second and third row of Fig. 9. However, it is important to note that the Monte Carlo time scale of the fluctuations we observe in the ordered regions, is dramatically larger than those related to the fluctuations in the disordered ones. Therefore, it does make sense to speak of ordered and disordered regions in these systems.

We then again turn to the question of the character of the vortex state in the disordered region and the possibility of a vortex liquid layer here. For this we use the modified helicity modulus $\tilde{\Upsilon}_z(R_1, R_2)$ and compare the results to the extended uniform system as we did for the cylindrical container. The results are shown in Fig. 10, where both rotating and non-rotating systems are considered. If one were to observe no appreciable difference in the temperature dependence of the helicity with and without rotation, one would conclude that the demarcation line seen in the images of Fig. 9 separates an ordered region from tension-less vortex tangle, with no discernible vortex liquid region.

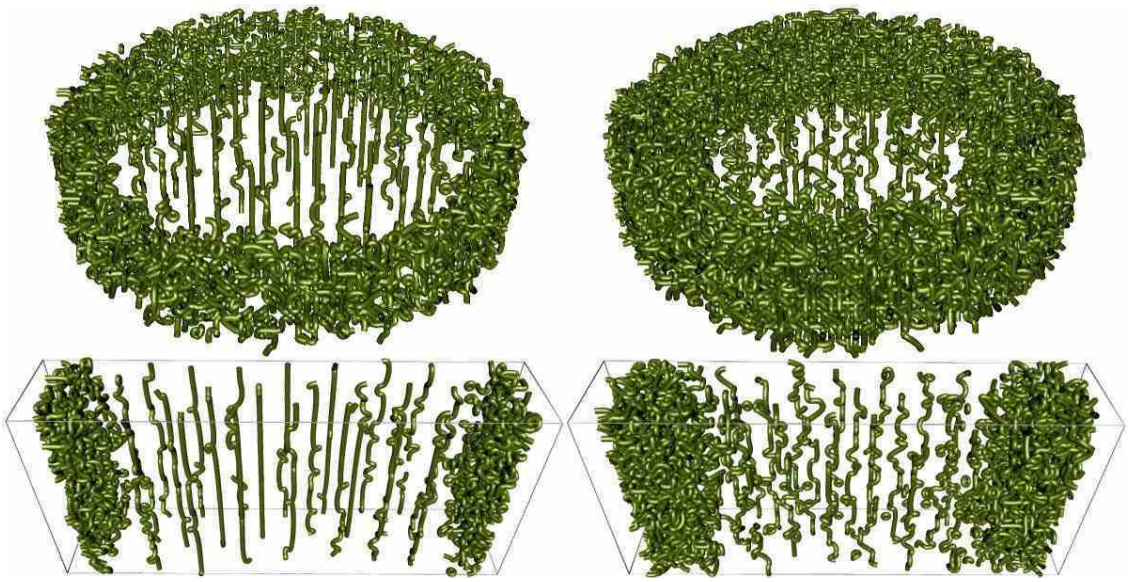

FIG. 8: (Color online) Snapshots of vortex configurations in a rotating trapped BEC at $T = 0.5$ (left figures) and at $T = 1.0$ (right figures). The top row shows a selection of 16 out of 72 layers in z direction. The bottom row shows smaller selections in the xy plane, but 32 out of 72 layers in z direction. Fluctuations are minimal in the trap center, and increase towards the edge of the trap. A distinct front separating regions of ordered and disordered vortices is easily identified.

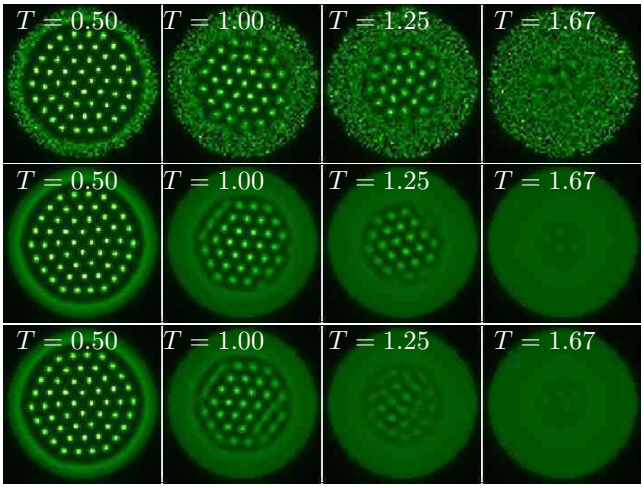

FIG. 9: (Color online) xy-positions of vortices in a trapped BEC integrated over z-direction. In the top row, we show snapshots, while the middle and bottom rows show averages of 10^5 and $5 \cdot 10^5$ MC sweeps, respectively. Every tenth configuration has been sampled. This provides information on the stability of the ordered region and the evolution of the disordered region as T varies.

The measurements indeed show that the presence of a rotation significantly reduces the temperature at which $\tilde{\Upsilon}_z$ vanishes. This reduction relative to the case of no rotation decreases with increasing R_1, R_2. That is, panel (d) is similar to panel (c) (no trap), whereas in panel (g) there is little difference between $\tilde{\Upsilon}_z(R_1, R_2)$ with and without rotation. Thus, for the latter case the presence of vortices essentially does not influence $\tilde{\Upsilon}_z$, and the destruction of superfluid density is driven by the proliferation of vortex loops. In panel (a) and (b) we have plotted $\tilde{\Upsilon}_z$ as a function of the distance $r_\perp = (R_1 + R_2)/2$ from the center of the trap for different temperatures. The same conclusions may be drawn here. For the largest $r_\perp$ there are small differences between (a) and (b), but closer to the center, the helicity modulus suddenly drops to zero when the temperature is increased in the system with rotation (b). This corresponds to the melting transition. The reason why we only find such characteristics in the central part, is that the density is almost uniform here. Further out, the density gradient is simply too large and the vortex line lattice crosses directly over to the tension-less tangle with no visible tension-full vortex liquid region in between. This is consistent with the experiments showing a very regular edge structure for systems with large number of vortices[42,43,44,45,46,47,58].

B. Anharmonic trap

Experimentally, the traps that are used to confine the Bose–Einstein condensates may also be made anharmonic[56]. To study the effect of a harmonic plus quartic trapping potential, we will use a modified Thomas–Fermi density distribution which varies in the xy-plane as $\alpha_1 + \alpha_2 {\mathbf{r}_\perp}^2 + \alpha_3 {\mathbf{r}_\perp}^4$. In an experiment with a rotating atomic gas, the ratio α_3/α_2 depends on the rotation frequency, but for technical reasons we cannot change Ω during the computations. Thus, we choose a fixed number of vortices by specifying f and vary only the temperature during computation runs for

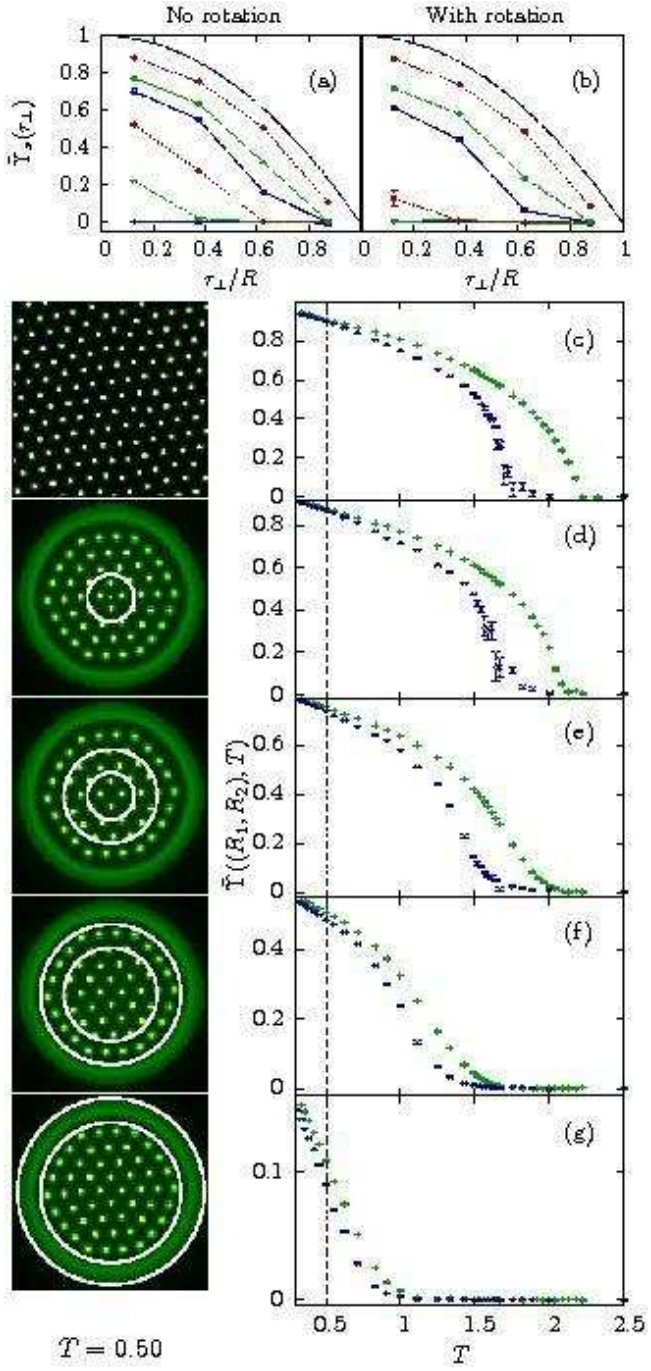

FIG. 10: (Color online) Results for $\tilde{\Upsilon}_z(R_1, R_2)$. The two top panels show computation results for the thermal depletion of the superfluid density in a harmonically trapped condensate ($r_\perp$ is the distance from the center of the trap) at the temperatures $T = 2.50$ (the lowermost curve), $T = 2.00$, $T = 1.67$, $T = 1.25$, $T = 1.00$, $T = 0.50$. The uppermost curve is the pure ground state density profile $P_{i\mu}$. In panels (c)–(g), the upper curve (+) is the helicity modulus without rotation, while the lower curve (×) the helicity modulus with rotation-induced vortices with filling fraction $f = 1/36$ as functions of temperature. Panel (c) shows Υ_z for a cubic uniform system with periodic boundary conditions. The remaining panels (d)-(g) show $\tilde{\Upsilon}_z(0, R/4)$, $\tilde{\Upsilon}_z(R/4, 2R/4)$, $\tilde{\Upsilon}_z(2R/4, 3R/4)$, and $\tilde{\Upsilon}_z(3R/4, R)$, respectively. The vortex plots on the left (obtained at $T = 0.50$) defines the radii R_1 and R_2 as white circles.

fixed α_3/α_2-ratios. To be precise, we have chosen the following density distribution $P_{i\mu} = P^a\left(\frac{r_{i\mu}}{R}\right)\ \Theta(R - r_{i\mu})$, where Θ is the Heaviside step function $\Theta(x) = 0, x < 0$, $\Theta(x) = 1, x > 0$, and

$$P^a(x) = \frac{4(1+\alpha)}{4(1+\alpha)+\alpha^2}\left\{1 + \alpha x^2 - (1+\alpha)x^4\right\}. \quad (19)$$

This ground state density profile has the property that its maximum is always unity. Consequently, the regions with the highest density should be comparable to both the uniform system and to the center of the harmonically trapped system at any given temperature. The value of α determines the shape of the density profile. Note that $\alpha = 0$ corresponds to a pure quartic trapping potential. We present results for this in the upper row of Fig. 12 for filling fractions $f = 1/36$ (left) and $f = 1/18$ (right). Such systems have a large density gradient close to the edge, but is on the other hand more uniform in the inner parts than the harmonic case. The effect is a scenario which fits in between the cylindrical case and the harmonically trapped system. There are slight angular distortions of the outermost vortices for $f = 1/36$, and an increased possibility for vortex lattice melting in the center as in an extended uniform system.

The generic ground state density profile $P_{i\mu}$ for the anharmonic trap is shown in Fig. 11, where the parameter α in Eq. (19) is taken to be $\alpha = 2$, such that the density profile has a distinct dip in the trap centre.

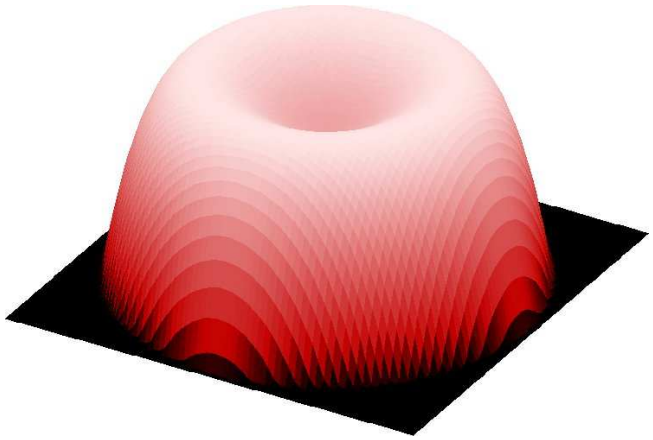

FIG. 11: (Color online) Radial density profile $P_{i\mu}$ for the case of an anharmonic trap with a local minimum of the ground state condensate density at the center of the trap.

In the second row of Fig. 12, we have chosen $\alpha = 2$ so that the density profile has a local minimum in the center. For low temperatures, the vortex configuration is close to that of the harmonic system, see Fig. 9. Then we notice a decreased visibility of the central vortices from around $T = 1.25$, a feature encountered in an experiment reported by Bretin and coworkers in 2004[56], where they increased the rotation frequency above the trap frequency. They speculated that this could be explained by

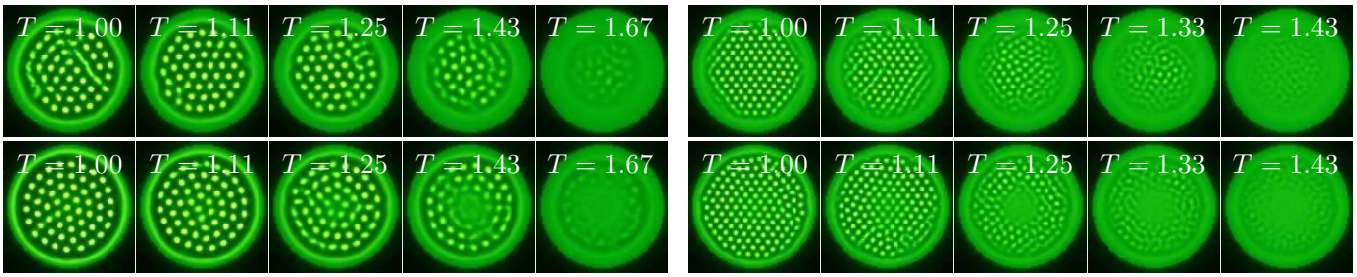

FIG. 12: (Color online) xy-positions of the vortices in a pure quartic trapping potential (top row) with filling fractions $f = 1/36$ (left) and $f = 1/18$ (right). In the second row, the vortices are trapped by a harmonic plus quartic potential, with $\alpha = 2$ in Eq. (19). Due to lower density, the visibility of the vortices close to the rotation axis is reduced for the highest temperatures. All images are averages over 100 000 Monte Carlo sweeps.

bending effects of the vortices. Our computations support this view.

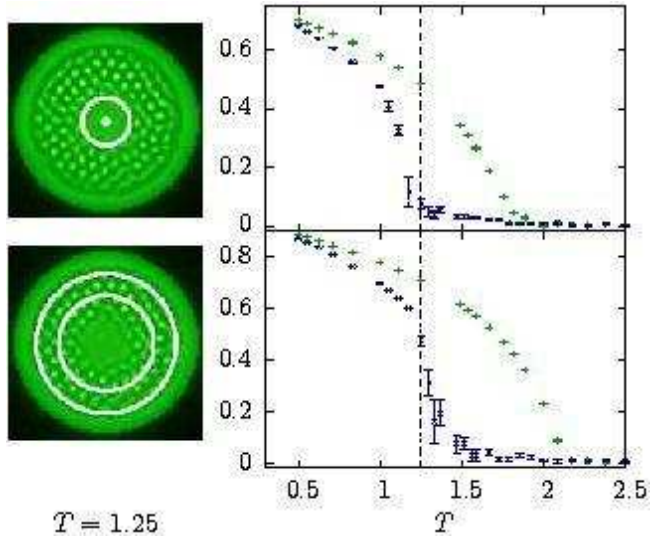

FIG. 13: (Color online) Results for $\tilde{\Upsilon}_z(R_1, R_2)$, comparing the low- and high-density regions in the top and bottom panels respectively. The lower curve ($\times$) in both panels, as well as the images on the left, are calculated for a system with filling fraction $f = 1/18$ and anharmonic density profile defined by $\alpha = 2$ (see Eq. (19)). Also included, are results for the same density profile, but with no rotation-induced vortices (upper curve, (+)).

Fig. 13 gives examples of the modified helicity modulus $\tilde{\Upsilon}_z(R_1, R_2)$ for two distinct regions of a system with $f = 1/18$ and $\alpha = 2$: One covering the region closest to the rotation axis, and one around the peak in the density. We have also included results for a non-rotating system, but with the same density profile. The vortex lines clearly forces $\tilde{\Upsilon}_z(R_1, R_2)$ to vanish in both regions for lower temperatures than without rotation, indicating a melting of the vortex line lattice. Additionally, we see that the region with the highest density remains in the vortex solid state up to higher T than the inner part. The central vortex line lattice melts easier because in this region there is a larger tendency for the vortex lines to have bending fluctuations due to the higher effective temperature, in the sense of Eq. (11).

VI. CONCLUSIONS

In this paper, we have considered thermal fluctuations of vortex matter in cylindrical traps with varying non-uniform model ground state densities of the condensate. As a benchmark we have also performed Monte Carlo computations of a uniform system and a cylindrical geometry with uniform ground state condensate density. We have in all cases taken care in ensuring that the helicity moduli in the direction *transverse* to the direction of rotation have vanished at temperatures well below the temperatures where the helicity moduli *along* the direction of rotation vanish. The purpose of this is to mimick, as well as possible, phase transitions in the BEC-vortex system *in a continuum* and to eliminate the artificial pinning effects that are inevitably present due to the numerical grid. Note however, that the model defined on a numerical grid could have a physical realization in terms of rotating Bose–Einstein condensates on an optical lattice. In such a system there is a real frustration of the vortex system due to commensuration effects. While this presents a very interesting problem in its own right, a study of such effects has not been the purpose of this paper.

Uniform system: In a uniform system, the 3D XY specific heat anomaly which the system exhibits in the absence of rotation, is rounded to a broad non-critical peak when rotation is present. This is the superfluid/BEC counterpart of the well-known finite-field remnant of the zero-magnetic field superconductor–normal metal transition when a superconductor is subjected to a finite magnetic field. In principle, it is also possible to extract a specific heat anomaly associated with the melting of the BEC-vortex lattice, although this has not been done in the present paper. The vortex fluctuations of importance

in this case are transverse phase fluctuations of the superfluid order parameter.

Uniform cylindrical confinement: In a cylindrical confinement with uniform ground state density profile, we have investigated the thermal fluctuations of the ordered vortex lattice in the confinement geometry as the temperature is increased. We find that the vortex lattice is first excited close to the circular edge of the confinement, and that the fluctuations in the vortex positions are directed along the perimeter of the cylinder. As the temperature is increased further, these ring-like thermal excitations creep inwards towards the center of the cylinder until the vortex lattice also at the center crosses over to a liquid phase. It is important that the inhomogeneity observed in the vortex fluctuations in this case is not due to the fact that the condensate effectively is warmer (in the sense of Eq. (11)) at the edge than at the center. The effective temperature is uniform throughout the system. The reason for the observed inhomogeneity of the fluctuations is that the local environment around each vortex is different at the edge than at the center. In particular, the vortex-vortex correlation effects that impede thermally assisted vortex motion are smaller at the edge than at the center. The coordination number of each vortex in the vortex lattice is larger at the center than at the edge. The corresponding interaction energies, and hence Coulomb barrier, that must be overcome to produce vortex motion, is therefore smaller at the edge of the confinement than at the center. Moreover, a transverse (angular) motion-pattern of the vortices are preferred compared to a radial motion-pattern, for the following reason. In a superfluid/BEC, the vortex interactions are unscreened (anti) Biot-Savart interactions. Therefore, the vortex ensemble constitutes an *incompressible* system in a superfluid/BEC. Hence, vortex motion is a collective process involving many vortices that have to be 'pushed' out of the way in order to pave the way for one vortex. Motion along the perimeter may be realized by moving all vortices in the *outermost ring* collectively, while radial motion involves a rearrangement of *all* vortices in the system. The former is obviously a collective process that is easier to accomplish than the latter. As a corollary, we may infer that this ring-like excitation pattern in a cylindrical confinement may change in the case of a *moderate type-II superconductor*, where effective screening of vortex interactions is a consequence of a fluctuating gauge field. This results in a compressible vortex system which to a much larger extent will allow radial as well as angular fluctuations in vortex positions.

Harmonic and anharmonic traps: For a Bose–Einstein condensate in a magnetic trap, we have focused on two types of trapping potentials, namely i) a harmonic trap giving a Thomas-Fermi ground state density profile of the BEC, and ii) an anharmonic trap in which we could vary the relative weights between a quartic and a quadratic term. The latter trap naturally leads to a modification of the inverse-parabolic Thomas-Fermi density profile, and in particular it is possible to induce a ground state superfluid density with a local minimum at the center of the trap. The thermally driven vortex-excitations in these systems are fundamentally different from the case of a uniform cylinder. The reason is that the vortex matter in the trapped BECs effectively have a highly non-uniform temperature, in the sense of Eq. (11). This is due to the rapidly decreasing density profile close to the edge, with a maximum effective temperature gradient at the edge of the trap. Hence, this promotes vortex-loop excitations as the edge of the trap is approached, thus inducing a vortex-matter phase where the line tension (free energy per unit length) of the vortex lines has vanished and the vortex lines effectively have lost their directionality in the direction of the rotation vector of the system. This gives a distinct region at the outer edge of the trap where vortex-loop induced violent vortex-line fluctuations wash out the image of each individual rotation-induced vortex line. This contrasts sharply with the images of ring-like collective directed vortex-line excitations in the uniform cylinder. The main difference between the harmonic and anharmonic trap is that for a harmonic trap the effective temperature of the system decreases monotonously towards the center of the trap, such that a monotonous evolution of the system from a vortex tangle to a vortex lattice at the center is observed when heated. For an anharmonic trap with a dip in the ground state condensate density at the center of the trap, we effectively have a local increase in the temperature of the system as the center of the trap is approached. Hence, we can have a tensionless vortex tangle at the center of the trap as well as at its edge. Our computations therefore provide a finite-temperature extension of the zero-temperature phase diagram for anharmonic traps presented in Ref. 59. According to Refs. 60,61, the experiment by Bretin et al.[56] takes place in the same regime, in which the density and interaction strength are too high to obtain a giant vortex with multiple quantization. We believe the experiment can be described by our model.

To summarize, we studied effects of density inhomogeneity and finite-size in a model system describing a trapped Bose–Einstein condensate. Although finiteness of the system and density inhomogeneity prohibit use of the notion of a true phase transition between different aggregate states of vortex matter (known to occur in three dimensional extended model systems), we find that nonetheless one can have various quasi-states of vortex matter surviving in a rather robust form at finite length scales in traps. Recent progress in Bose–Einstein condensates has resulted in the availability of systems with various symmetries and multiple components where one can anticipate new states of vortex matter. This study suggests that predictions of a theory based on a uniform density might nonetheless have rather robust finite-size realizations in actual inhomogeneous trapped systems.

Acknowledgments

This work was supported by the Research Council of Norway, Grant Nos. 158518/431, 158547/431 (NANOMAT), 167498/V30 (STORFORSK), the National Science Foundation, Grant No. DMR-0302347, Nordforsk Network on Low-Dimensional Physics. SK and EB acknowledges the hospitality of the Center for Advanced Study at the Norwegian Academy of Science and Letters, where part of this work was done.

[1] I. R. Coddington, *Vortices in a Highly Condensed Bose Gas*, PhD Thesis, University of Colorado, (2004).
[2] M. Greiner, *Ultracold quantum gases in three-dimensional lattice potentials*, PhD thesis, Ludwig Maximilians Universität Muenchen, Germany (2003).
[3] C. Regal, *Experimental realizations of BCS-BEC crossover physics with a Fermi gas of atoms*, PhD thesis, University of Colorado (2005).
[4] M. W. Zwierlein, *High-Temperature Superfluidity in an Ultracold Fermi Gas*, PhD Thesis, Massachusetts Institute of Technology, (2006).
[5] J. M. Kosterlitz and D. J. Thouless, J. Phys. C **6**, 1181 (1973); J. M. Kosterlitz, J. Phys. C **7**, 1084 (1974); *ibid*, **10**, 3753 (1977).
[6] For a thorough and comprehensive statistical mechanical treatment of the metal-insulator transition in the 2D Coulomb gas, with particular emphasis on the difficult problem of treating the screening properties in the critical region, see J. S. Høye and K. Olaussen, Physica **104A**, 447 (1980); *ibid*, **107A**, 241 (1981).
[7] H. Kleinert, Lett. Nuovo Cimento, **35**, 409 (1982).
[8] Z. Tesanovic, Phys. Rev. B **51**, 16204 (1995); *ibid*, B **59**, 6449 (1999).
[9] A. K. Nguyen and A. Sudbø, Phys. Rev. B **57**, 3123 (1998); *ibid*, B **58**, 2802 (1998).
[10] A. K. Nguyen and A. Sudbø, Phys. Rev. B **60**, 15307 (1999); Europhys. Lett. **46**, 780 (1999). See also A. K. Nguyen, R. E. Hetzel, and A. Sudbø, Phys. Rev. Lett., **77**, 1592 (1996).
[11] H. Kleinert, *Gauge Fields in Condensed Matter Physics, Vol. 1*, World Scientific, Singapore 1989.
[12] K. Fossheim and A. Sudbø, *Superconductivity: Physics and Applications*, John Wiley & Sons, Ltd (2004), see Chapters 9,10.
[13] The 1949 discussion remark of L. Onsager is well worth quoting here: "Finally, we can have vortex rings in the liquid and the thermal excitation of He II, apart from phonons, is presumably due to vortex rings of molecular size. As a possible interpretation of the λ-transition, we can understand that when the concentration of vortices reaches the point where they form a connected vortex tangle throughout the liquid, then the liquid becomes normal." L. Onsager, Nuovo Cimento Suppl., **249** , (1949). This idea was first put on a quantitative footing in 2D in Refs. 5, and in 3D in Refs. 7,8,9,10. In particular, see Fig. 3 of A. K. Nguyen and A. Sudbø, Phys. Rev **B** 60, 15304 (1999).
[14] J. Hove, S. Mo, and A. Sudbø, Phys. Rev. Lett., **85**, 2368 (2000).
[15] P. W. Anderson, *Basic Notions in Condensed Matter Physics*, Benjamin Cummings, London (1984).
[16] W. Ketterle, K. B. Davis, M. A. Joffe, A. Martin, and D. E. Pritchard, Phys. Rev. Lett., **73**, 2253 (1995); K. B. Davis, M. -O. Mewes, M. R. Andrews, N. J. van Druten, D. S. Durfee, D. M. Kurn, and W. Ketterle, Phys. Rev. Lett. **75**, 3969 (1995)
[17] W. Petrich, M. H. Anderson, J. R. Ensher, and E. A. Cornell, Phys. Rev. Lett., **74**, 3352 (1995); M. H. Anderson, J. R. Ensher, M. R. Matthews, C. E. Wieman, and E. A. Cornell, Science, **269**, 198 (1995).
[18] C. C. Bradley, C. A. Sackett, and R. G. Hulet, Phys. Rev. Lett., **78**, 985 (1997).
[19] M. R. Matthews, B. P. Anderson, P. C. Haljan, D. S. Hall, C. E. Wieman, and E. A. Cornell, Phys. Rev. Lett. **83**, 2498 (1999).
[20] C. Raman, M. Köhl, R. Onofrio, D. S. Durfee, C. E. Kuklewicz, Z. Hadzibabic, and W. Ketterle, Phys. Rev. Lett. **83**, 2502 (1999).
[21] M. Snoek and H. T. C. Stoof, Phys. Rev. Lett. **96**, 230402 (2006).
[22] M. Snoek and H. T. C. Stoof, Phys. Rev. A **74**, 033615 (2006).
[23] M. M. Parish, S. K. Baur, E. J. Mueller, and D. A. Huse, `arXiv:0709.1120`, (2007).
[24] E. Babaev, A. Sudbø, and N. W. Ashcroft, Nature, **431**, 666 (2004).
[25] S. Kragset, E. Babaev, and A. Sudbø, Phys. Rev. Lett., **97**, 170403 (2006).
[26] A. J. Leggett, Rev. Mod. Phys., **73**, 307 (2001), and references therein.
[27] E. H. Brandt, Prog. Phys. **58**, 1465 (1995).
[28] M. Greiner, C. A. Regal, and D. S. Jin, Nature **426**, 537 (2003).
[29] C. A. Regal, M. Greiner, D. S. Jin, Phys. Rev. Lett. **92**, 040403, (2004).
[30] M. W. Zwierlein, C. H. Schunck, A. Schirotzek, and W. Ketterle, Nature, **442**, 54 (2006).
[31] Y. Shin, M. W. Zwierlein, C. H. Schunck, A. Schirotzek, and W. Ketterle, Phys. Rev. Lett. **97**, 030401 (2006).
[32] C. H. Schunck, M. W. Zwierlein, A. Schirotzek, and W. Ketterle, Phys. Rev. Lett. **98**, 050404 (2007).
[33] C.H. Schunck, Y. Shin, A. Schirotzek, M.W. Zwierlein, and W. Ketterle, Science, **316**, 867 (2007).
[34] R. E. Hetzel, A. Sudbø, and D. A. Huse, Phys. Rev. Lett. **69**, 518 (1992).
[35] T. Chen and S. Teitel, Phys. Rev. B **55**, 15197 (1997).
[36] X. Hu, S. Miyashita, and M. Tachiki, Phys. Rev. Lett. **79**, 3498 (1997).
[37] P.Olsson and S. Teitel, Phys. Rev. Lett. **80**, 1964 (1998).
[38] S. Ryu and D. Stroud, Phys. Rev. B **57**, 14476 (1998).
[39] G. Baym and C. J. Pethick, Phys. Rev. Lett., **76**, 6 (1996).
[40] G. Watanabe, G. Baym, and C. J. Pethick, Phys. Rev. Lett., **93**, 190401 (2004).
[41] N. R. Cooper, S. Komineas, and N. Read, Phys. Rev. A **70**, 033604 (2004).
[42] K. W. Madison, F. Chevy, W. Wohlleben, and J. Dalibard, Phys. Rev. Lett., **84**, 806 (2000).
[43] I. Coddington, P. Engels, V. Schweikhard, and E. A. Cor-

nell, Phys. Rev. Lett., **91**, 100402 (2003).
[44] V. Schweikhard, I. Coddington, P. Engels, V. P. Mogendorff, and E. A. Cornell, Phys. Rev. Lett., **92**, 040404 (2004).
[45] N. L. Smith, W. H. Heathcote, J. M. Krueger, and C. J. Foot, Phys. Rev. Lett., **93**, 080406 (2004).
[46] I. Coddington, P. C. Haljan, P. Engels, V. Schweikhard, S. Tung, and E. A. Cornell, Phys. Rev. A **70**, 063607 (2004).
[47] S. R. Muniz, D. S. Naik, and C. Raman, Phys. Rev. A **73**, 041605 (2006).
[48] N. Metropolis, A. W. Rosenbluth, M. N. Rosenbluth, A. H. Teller, and E. Teller, J. Chem. Phys., **21**, 1087 (1953).
[49] W. K. Hastings, Biometrika, **57**, 97 (1970).
[50] The resulting phase where one has zero helicity moduli in the direction transverse to the rotation vector, concomitant with a finite helicity modulus parallell to the rotaton vector, may be dubbed a "floating solid phase", since the vortex lattice "floats" as a solid while being thermally depinned from the numerical grid. Going to low enough filling fraction to avoid artificial pinning of the vortex lattice to the numerical grid, is a minimum requirement for studying phase transitions in vortex lattices in continuum systems. There are, however, interesting physical situations where one really has a rotating BEC defined on a discrete lattice system, most notably an optical lattices. (See for instance, H. Pu, L. O. Baksmaty, and N. P. Bigelow, Phys. Rev. Lett., **94**, 190401 (2005); S. Tung, V. Schweikhard, and E. A. Cornell, Phys. Rev. Lett., **97**, 240402 (2006).) In this case, one has competing length scales in the system, with associated competing energy scales. While this poses an extremely interesting problem, both in 2D as well as in 3D systems, it is beyond the scope of the present work.
[51] M. Campostrini, M. Hasenbusch, A. Palisetto, P. Rossi, and E. Vicari, Phys. Rev B **63**, 214503 (2001).
[52] For a comprehensive review on the Abrikosov vortex lattice in type-II superconductors in a magnetic field, see G. Blatter, M. V. Feigel'man, V. B. Geshkenbein, A. I. Larkin, and V. M. Vinokur, Rev. Mod. Phys., **66**, 1125 (1994).
[53] S. A. Gifford and G. Baym, Phys. Rev. A **70**, 033602 (2004).
[54] L. J. Campbell and R. M. Ziff, Phys. Rev. B **20**, 1886 (1979).
[55] Yu. Lozovik and E. Rakoch, Phys. Rev. B **57**, 1214 (1998).
[56] V. Bretin, S. Stock, Y. Seurin, and J. Dalibard, Phys. Rev. Lett. **92**, 050403 (2004).
[57] J. R. Abo-Shaeer, C. Raman, and W. Ketterle, Phys. Rev. Lett. **88**, 070409 (2002).
[58] J. R. Abo-Shaeer, C. Raman, J. M. Vogels, and W. Ketterle, Science **292**, 476 (2001).
[59] G. M. Kavoulakis and G. Baym, New Journal of Physics **5**, 51.1 (2003).
[60] A. D. Jackson, G. M. Kavoulakis, and E. Lundh, Phys. Rev. A **69**, 0536619 (2004).
[61] A. D. Jackson and G. M. Kavoulakis, Phys. Rev. A **70**, 023601 (2004).